Performance study of a thin film cation exchange membrane on carbon electrode for supercapacitor application

Electrochimica Acta 468 (2023) 143143

Contents lists available at ScienceDirect

Electrochimica Acta

journal homepage: www.journals.elsevier.com/electrochimica-acta

Performance study of a thin film cation exchange membrane on carbon electrode for supercapacitor application

Davide Molino [a,*], Alessandro Pedico [a,b], Pietro Zaccagnini [a,b], Sergio Bocchini [a,b], Andrea Lamberti [a,b]

[a] Politecnico di Torino, Dipartimento di Scienza Applicata e Tecnologia (DISAT), Corso Duca degli Abruzzi, 24, Torino 10129, Italy
[b] Istituto Italiano di Tecnologia, Center for Sustainable Future Technologies, Corso Trento, 21, Torino 10129, Italy

ARTICLE INFO

Keywords:
SPEEK
Supercapacitor
Cation exchange membrane
Activated carbons

ABSTRACT

In this work we report a green procedure for the infiltration of a SPEEK solution into a porous carbon electrode resulting in a thin-film cation exchange membrane. The electrodes have been investigated by a morphological point of view, showing the formation of a thin coating infiltrated into the porous carbonaceous matrix, while mechanical peeling of a tape demonstrated the adhesion of the proposed layer. The fabricated electrodes have been analyzed by electrochemical measurement. The 3-electrode cyclic voltammetry measurements allowed to verify the voltage window resulting in an improved negative potential, while the electrochemical impedance spectroscopy showed a reduction of the electrical resistance. The SPEEK electrode was used in a supercapacitor and deeply characterized by electrochemical analysis. The reported findings demonstrate for the first time the possibility to exploit a cation exchange material in thin film configuration for supercapacitor application with improved performance of the device and exclusively involving the use of nontoxic reagents.

1. Introduction

Ion exchange membranes (IEMs) are attracting increasing interest in the scientific community [1]. IEMs find applications in many fields, like the chemical industry [2], water desalination [3], energy harvesting [4] and energy storage [5]. In recent years, IEMs have been widely studied for applications in which it is required to separate anions from cations, allowing the passage of one species while rejecting the other. Their unique properties of selectivity towards charged species present in solution have made them popular in the field of separation. The chemistry of these membranes is extremely variable, however, most of them are still based on ionic polymers: a type of polymer that contain both covalent and ionic bonds in their molecular structure. These polymers can be either organic or inorganic, and this combination of bond types is the key feature that distinguishes them from traditional polymers [6]. The structure of IEMs is constituted by ionic polymers to which ionizable groups are covalently bound. These groups dissociate in presence of water, leaving charged groups bound to the matrix which are responsible for the charge selectivity. The ion exclusion is described in thermodynamics terms by the Gibbs–Donnan equilibrium [7]. The consequence is that IEMs can convey a high flux of ions through their structure. This can happen in the presence of a concentration gradient or with an applied electric field. The latter is the typical case of an electrochemical device in which IEMs are employed to boost performance. In 2014, Chen et al. [8] employed a cation exchange membrane to reduce the self-discharge observed in their supercapacitors, mainly caused by the shuttling of anion species in the electrolyte. They substituted the separator between the electrodes with a commercial Nafion membrane, with the aim of allowing only the passage of H^+ ions. The results showed a net reduction of the self-discharge current, thus obtaining a device with improved stability over time. In 2018, Paleo et al. [9] proposed again to employ a Nafion membrane, in this case exchanged with Na^+ ions. Its purpose was to work as a separator in a flexible supercapacitor designed for textile applications. The presence of the membrane not only ensured flexibility, but it was also responsible for the low discharge current and the long cycling stability. In 2020, Guo et al. [10] synthesized and characterized an anion exchange membrane specifically designed to work as a separator in a supercapacitor, showing excellent chemical resistance, high hydroxide conductivity, and good cycling performance of the device. In this case, the membrane was working as an electrolyte itself, holding water molecules inside its structure, enabling a fast movement of OH^- ions and preventing the

* Corresponding author.
E-mail address: davide.molino@polito.it (D. Molino).

https://doi.org/10.1016/j.electacta.2023.143143
Received 31 December 2022; Received in revised form 29 August 2023; Accepted 2 September 2023
Available online 6 September 2023

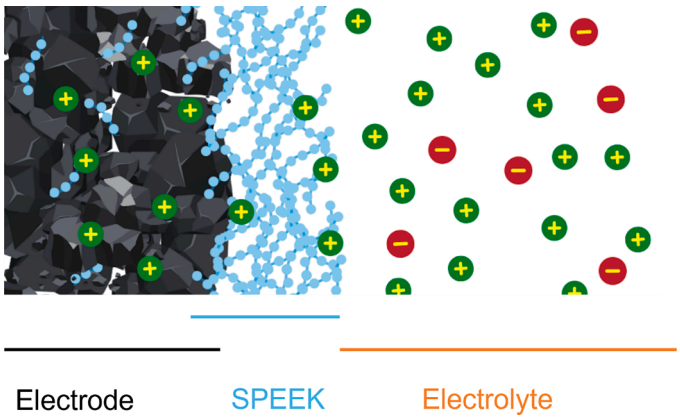

Fig. 1. Schematic composition of the electrode: SPEEK is mixed with activated carbon and used as binder. Over the electrode is depicted a thin film of IEM which provides ionic selectivity.

evaporation of water even at high temperatures. In 2022, Cai et al. [11] successfully fabricated an anion exchange membrane for application in Zn-air batteries, boosting the stability of the battery and enlarging its operating voltage window. In all the previous works, the presence of the IEM is a key point for improving the performance of the device. However, there are drawbacks related to the exploitation of such membranes inside an electrochemical energy storage device. While strongly reducing the self-discharge phenomena, they are also responsible for the increase of the electrical resistance of the cell. This behavior is observed in all the previously cited works, and it is well-known in the field of electro-membrane processes [12]. This consequently leads to the decrease of the energy efficiency of the device and thus must be avoided as much as possible.

Poly(ether ketone) (PEEK) is a high-performance engineering thermoplastic with excellent solvent resistance, thermo-oxidative stability, and mechanical properties. Its sulfonated derivatives provide a cost-effective alternative to Nafion membranes [13]. The aromatic backbone of PEEK contributes to its thermal and mechanical stability and allows for chemical modification through electrophilic substitution, such as sulfonation. IEM based on sulfonated poly(ether ketone) (SPEEK) are well-known in literature [14–16]. Sulfonated polymers are also used in solid state capacitors: as suggested by Rajaputra and Karaman [17,18], it is possible to exploit the sulfonation of an hydrogel made of polyvinyl alcohol to enhance the ionic conductivity and improve the performance of the device.

In this work, we reported the employment of a cation exchange membrane in a supercapacitor based on activated carbons (AC) working with an aqueous electrolyte (Fig. 1). SPEEK was selected for this purpose. A very thin layer of IEM (<700 nm) composed by SPEEK was coated on the top of the AC to boost the electrochemical performance of the supercapacitor while contemporarily avoiding any increase in internal electrical resistance thanks to its controlled thickness and conformal coating, perfectly matching the features of the AC beneath. The preparation of the electrodes and the coating procedure were performed with a fully scalable approach, exclusively involving the use of nontoxic reagents. In addition, the feasibility of using SPEEK as a binder for AC based electrodes was also studied.

2. Experimental

2.1. Sample preparation

All the electrodes tested were composed of an active material deposited over a 20 μm thick titanium current collector purchased from Goodfellow. The active material was produced by mixing in dimethyl sulfoxide (DMSO, ≥99%, from Merck) in an amount of 90% wt. activated carbon (YP-50F, provided by Kuraray) and 10% wt. polyvinylidene fluoride (PVDF, M_w 534000, from Merck) as the binder. An alternative preparation was made exploiting the SPEEK as the binder, in the same percentage. The slurries obtained in this way were sonicated for 30 min using a frequency of 40 kHz in an ultrasonic bath (BRANSON 3800 CPXH) and stirred overnight at room temperature. To obtain the final electrodes, the titanium foils were coated with the slurry using a doctor blade method, to obtain a controlled thickness of the coated film of around 100 μm. The foils were dried at 60 °C overnight and then cut in a circular shape using a pulsed nanoseconds fiber laser, emitting with a wavelength of 532 nm. The cut was performed using a power of 6.5 W and a scan velocity of 25 mm s^{-1}. The final electrodes had a thickness of 65 μm of active material and a mass loading of about 5 mg cm^{-2} (Fig. 2).

The SPEEK was prepared by dissolving 8 g of polyether ether ketone (M_w 20800, from Merck) in 50 mL of sulfuric acid (95–97%, from Merck). The polymer slowly dissolved forming a red viscous solution. After 96 h the solution was slowly added dropwise in a large excess of cold deionized water (DI H_2O). After standing overnight, the precipitate was filtered and washed several times with DI H_2O and thus dried at

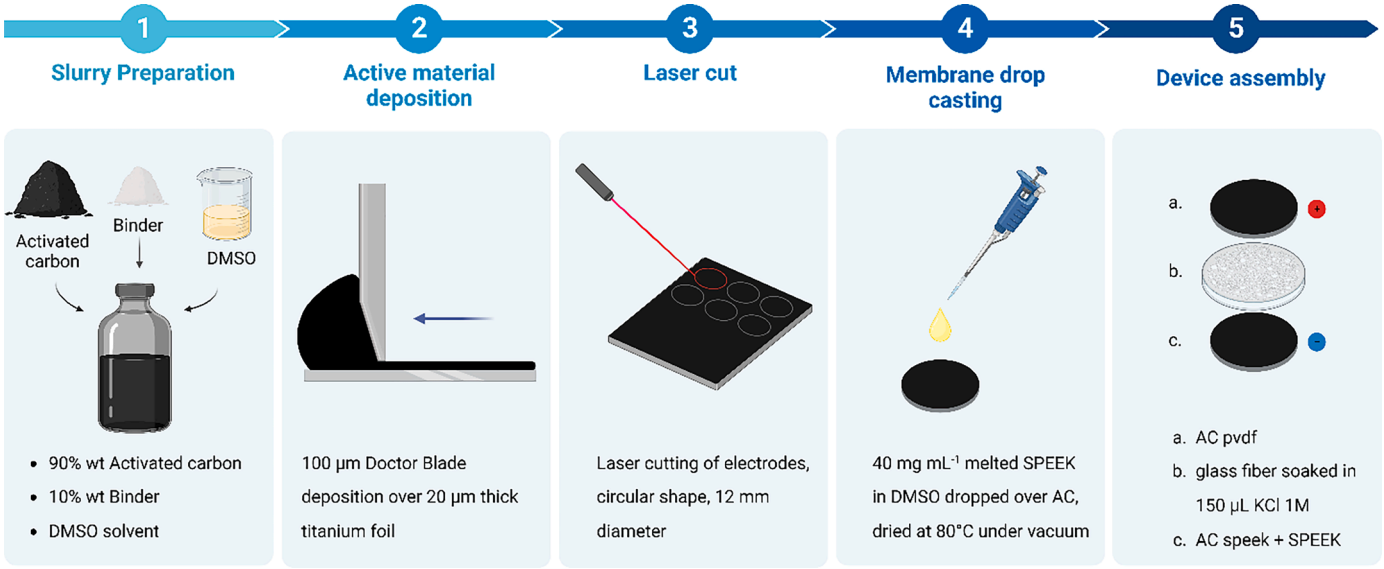

Fig. 2. Flowchart of electrodes and device production process.

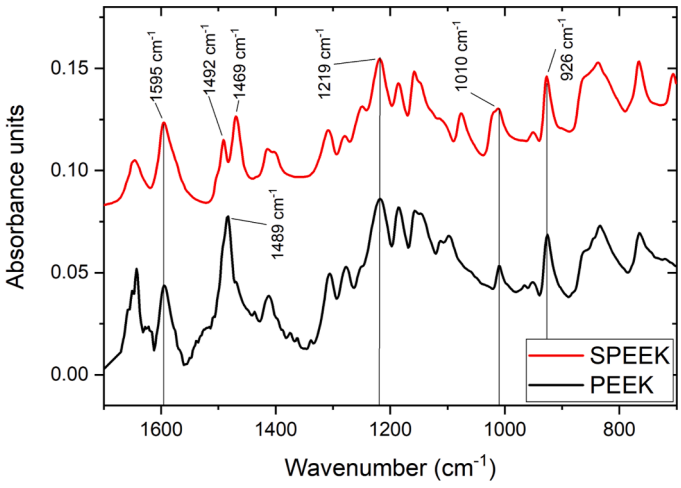

Fig. 3. ATR-IR spectra of SPEEK.

60 °C in a vacuum oven until constant weight.

The SPEEK was subsequently immersed in potassium chloride (KCl, ≥99%, from Merck) 1 M overnight in order to exchange the H^+ of the sulfonic group with the K^+. After washing in DI H_2O, the SPEEK was dispersed in DMSO to obtain a concentrated solution suited for drop-casting applications, with a final concentration of 40 g L^{-1}.

Approximately one-third of PVDF binder-based electrodes and one-third of the SPEEK binder-based electrodes underwent a process of deposition of the SPEEK over the activated material. This was carried out by drop-casting 40 μL cm^{-2} of the SPEEK solution on each electrode, immediately followed by a drying step at 80 °C in low vacuum condition for 1 h in a glass oven (B-585, from Büchi).

2.2. Characterizations

Electron microscopy characterization was carried out with a Field-Emission Scanning Electron Microscope (FESEM Supra 40, manufactured by Zeiss) equipped with a Si(Li) detector (Oxford Instruments) for Energy-Dispersive X-ray (EDX) spectroscopy.

Fourier Transform Infrared (FTIR) spectroscopy (Bruker Tensor II) was performed on the material in attenuated total reflection (ATR) configuration.

Electrochemical tests were conducted both in half-cell configuration (3-electrodes) and in device configuration (2-electrodes). The first type of analysis was performed in a Swagelok T-cell, employing 12 mm diameter electrodes. The separator was the GF/D glass fiber (675 μm, from Whatman). The reference was an Ag/AgCl 3 M KCl electrode. The WE was produced as previously explained, while the CE was prepared by mixing 85% wt. activated carbon (YP-50F), 5% wt. carbon black (Timical C65, from Imerys) and 10% wt. PTFE (60% wt. dispersion in H_2O, from Merck) in ethanol (≥99%, from Merck). The slurry was dried until it got the consistency of a dough, flattened, resulting in a dense and thick layer. The layer was cut in a circular shape to obtain a disk of 12 mm in diameter. The disk was dried at 60 °C overnight. This preparation results in a 1 mm thick stand-alone electrode. Galvanostatic device measurements were performed using the same Swagelok T-cells. The aging measurements were performed with standard 2032 coin cells from MTI. The separator was the previously mentioned GF/D from Whatman. Coin cells were closed with a digital pressure electric crimper (MSK-160E, from MTI) applying a pressure of 3 MPa. For all the cells, the electrolyte was KCl 1 M.

On the above-described cells, operative voltage measurements (OVM) were performed by repeating anodic and cathodic voltammetric scans at relatively low scan rates of 5 mV s^{-1} of increasing polarization levels of 0.1 V from 0 V vs open circuit potential (OCP) to ±1 V vs OCP. In device configuration, impedance spectroscopy measurements were performed by applying a sinusoidal signal with V_p = 10 mV and

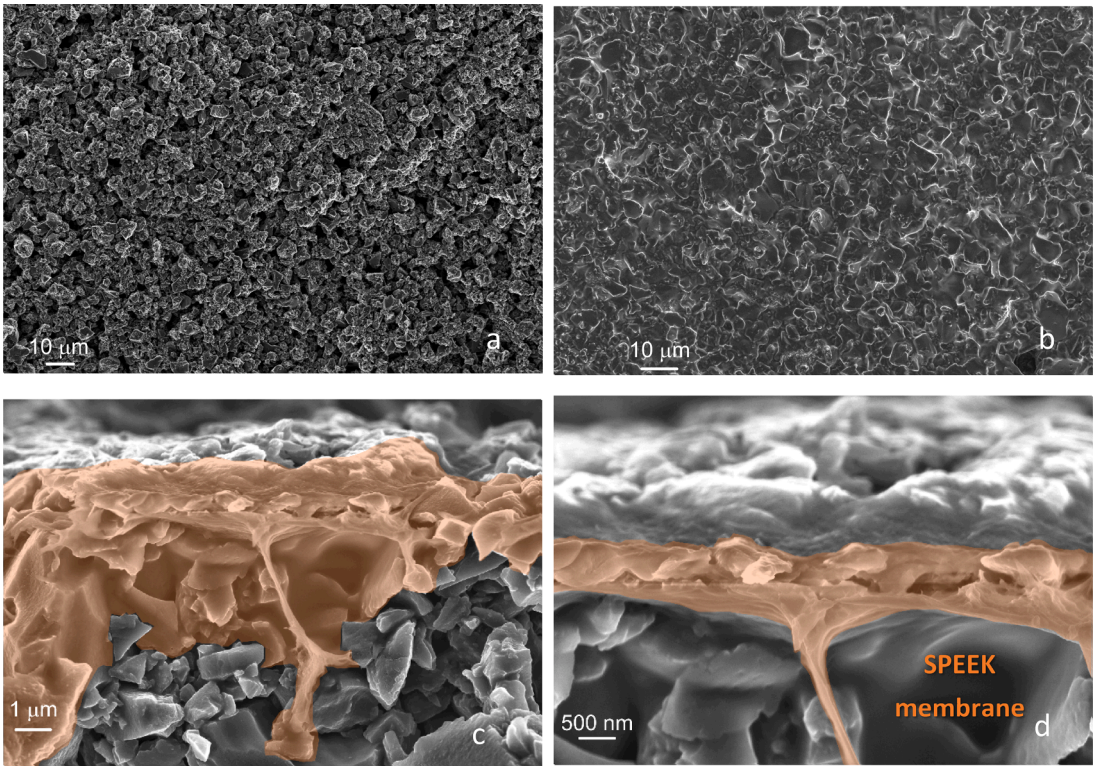

Fig. 4. FESEM images of AC: a) top view of bare AC, b) top view of AC coated with SPEEK, c) Cross section of coated AC: orange shaded SPEEK membrane and its penetration among AC, d) Detail of SPEEK membrane cross section.

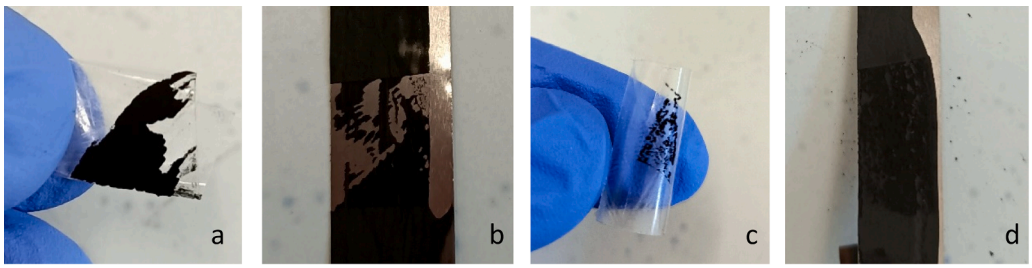

Fig. 5. a), b) PVDF binder-based slurry over Titanium, c), d) SPEEK binder-based slurry over Titanium.

frequency ranging from 1 MHz to 10 mHz. Cyclic voltammetry characterization was performed using a scan rate of 5 mV s^{-1} between 0 V and 800 mV.

The electrochemical measurements were performed with a VMP3 potentiostat provided by Bio-Logic. This instrument offers a potential range of ±10 V, a maximum current of 400 mA, with a resolution of 50 μV and 760 pA. The accuracy is declared to be <0.1% of the full-scale range. The electrometer has an input impedance greater than 1 TΩ, a capacitance of less than 20 pF, and a bias current lower than 5 pA.

3. Results and discussion

3.1. ATR-IR characterization

As shown in Fig. 3, the aromatic C—C band peak at 1489 cm^{-1} in PEEK is split into 1492 and 1469 cm^{-1} in SPEEK due to the substitution resulting from the sulfonation reaction. The peak at 1080 cm^{-1} corresponds to the asymmetric stretching vibrations of the sulfonation reaction. In the spectrum, the classical PEEK absorptions are observed at 1595 cm^{-1} (C═O stretch), 1219 cm^{-1} (pH—CO-pH stretch), 1010 cm^{-1} (C—O-C or C—O stretch), and 926 cm^{-1} (symmetric pH-(C═O)-pH stretch). Absorption due to aromatic sulfonic groups is also observed at 1020 cm^{-1} (symmetric SO_3H stretch).

3.2. FESEM characterizations

Electron microscopy was employed to study the morphology of the AC samples, both with and without the IEM coating. In Fig. 4b, it is possible to appreciate the uniformity of the coating on a very large area. The SPEEK coating is homogenous on the whole sample, proving the effectiveness of the coating method in providing a uniform, thin and conformal coating on the whole AC surface. The thickness of the SPEEK coating ranges between 600 nm and 700 nm (Fig. 4d), much thinner than common IEMs. The maximum depth reached by the SPEEK is 5 μm (Fig. 4c). The morphology of the AC beneath is not affected by the presence of the SPEEK coating, which is perfectly mimicking the pattern.

3.3. Adhesion tests

The first characterization was the evaluation of the adhesion performance of both the PVDF binder-based and the SPEEK binder-based slurries on titanium. It was chosen to test this feature by performing an adhesion evaluation experiment. This kind of analysis consisted in a "peeling-like" test. A tape was sticked over the active materials and then the adhesive strip was stripped away. By visual inspection it is possible to evaluate which material has the best adhesive properties, as also done in [19–22].

Comparing the results of these tests, it is clear that the SPEEK binder-based slurry has a much more adhesive ability compared to PVDF binder-based slurry. The amount of active material taped to the strip in the case of the SPEEK is negligible compared to the PVDF (Fig. 5). Examining the substrate, it is also possible to see that the test left the titanium collector totally exposed in the case of the PVDF, while the coverage was maintained for the SPEEK case.

3.4. Three electrodes electrochemical characterization

In this section, all electrodes proposed were tested and analyzed through 3-electrodes measurements to study their properties singularly. The electrodes tested are: 2 not covered electrodes, the first bonded to Ti substrate through classic PVDF binder (AC pvdf), the other one was bonded with SPEEK instead of PVDF (AC speek). Both of them were then covered with melted SPEEK and tested again (respectively AC pvdf + SPEEK and AC speek + SPEEK). The impedance spectroscopy was

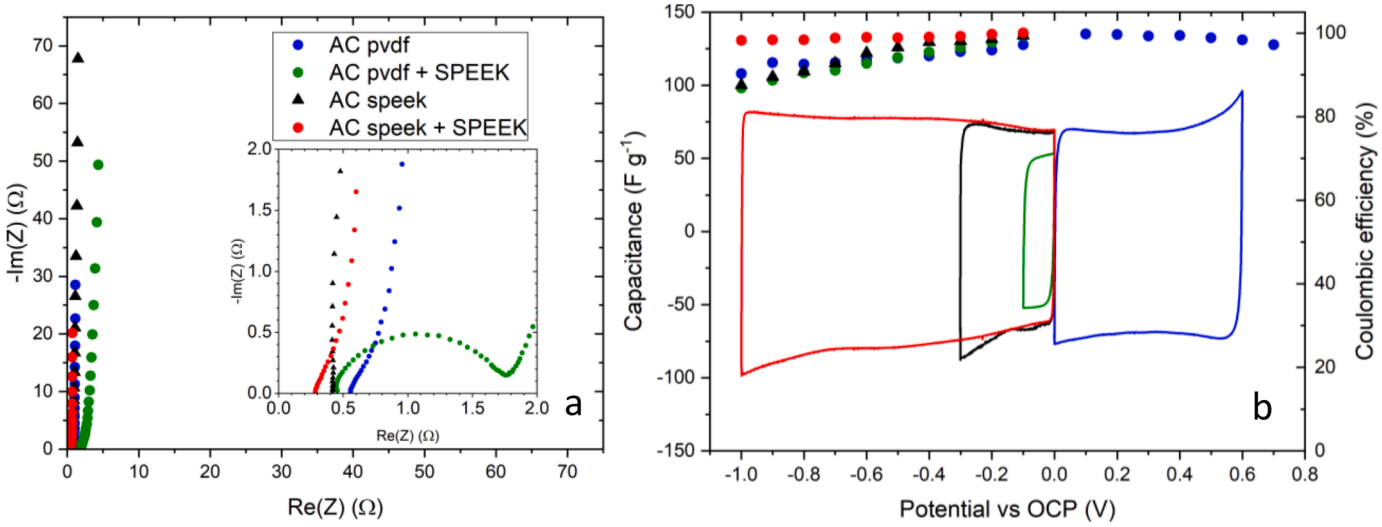

Fig. 6. 3-electrodes measurement comparison of all different electrodes taken into account. a) impedance spectroscopy, b) cyclic voltammetry.

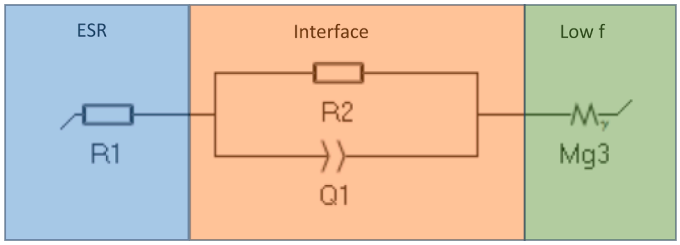

Fig. 7. Equivalent circuits used to fit the impedance spectroscopies of each electrode.

performed on each electrode after a 2-h open circuit relax time (following the assembly of the measurement setup) and right before the performance of the cyclic voltammetry required to evaluate the operative voltage window of the electrode. Cyclic voltammetry, on the other hand, where performed between 0 V vs OCP and +1/−1 V vs OCP with step of 100 mV. Anodic and cathodic scans were performed on different electrodes, in order to decouple the measurements. During each step, the cyclic voltammetry was repeated at least 50 times. In Fig. 5b it is reported the shape of CV related to the maximum OVM (continuous line) and the coulombic efficiency related to each voltage step (dots on the upper part of the graph). For all the other not displayed curves, see supporting information.

In Fig. 6 the 3-electrodes electrochemical characterizations are reported. Coulombic efficiency is evaluated from cyclic voltammetries as the ratio between the charge provided to the electrode during the charging step of the measurement and the charge the electrode was able to return during the discharge process. The charge was evaluated by integrating the current in the time as follows: $Q_c = \int_0^{T_{cycle/2}} Idt$ and $Q_d = \int_{0T_{cycle/2}}^{T_{cycle}} Idt$, where $Q_{c/d}$ is the charge in charging/discharging, I is the current and T_{cycle} is the total time of a single cycle of CV. It is possible to tell charge from discharge only from the time, since the cyclic voltammetry is performed at a constant scan rate, so the division between charge and discharge is placed at $T_{cycle}/2$.

Considering the electrochemical impedance spectroscopies, all obtained Nyquist plot were fitted exploiting a 7-parameter equivalent circuit able to take into account the equivalent series resistance, the interface contribution and finally the diffusive layer and the behavior at low frequencies. The circuit is depicted in Fig. 7.

The corresponding transfer function is the following:

$$Z(f) = R_1 + R_2 // \frac{1}{Q_1(j2\pi f)^{\alpha_1}} + R_{d1}\frac{\coth(j\tau_{d1}2\pi f)^{\gamma_1/2}}{(j\tau_{d1}2\pi f)^{1-\gamma_1/2}}$$

It was decided to exploit 2 resistive components (R_1 and R_2), a constant phase element (Q_1) and an anomalous diffusion element (M_{g3}). Moreover, this circuit behaves in the same way of the one proposed by Dsoke et al. [23]. For data extracted from the fitting, see supporting informations, Section 3s. The results of the impedance spectroscopy (Fig. 6a) show how substituting the PVDF (marked in blue and labeled "AC pvdf") with the SPEEK (marked in black and labelled "AC speek") leads to a reduction of the ESR. In the cyclic voltammetry plot, only curves with coulombic efficiency greater than 98% are reported. The addition of the SPEEK (both as a membrane and as a binder) allows the activated carbon electrode to work at negative potentials with a coulombic efficiency greater than 98%, while in the AC pvdf case this was not possible (@ −0.1 V, coulombic efficiency = 97%) (Fig. 6b). In the case of the AC coated with the SPEEK, it is possible to observe a decrease in the specific capacitance, happening for both the PVDF-based electrode and the SPEEK-based one (marked respectively in red and green, labeled AC pvdf + SPEEK and AC speek + SPEEK). By looking at the coulombic efficiency, when combining the SPEEK used as a binder with the SPEEK used as IEM coated over the AC, the electrodes behave more efficiently (Fig. 6b), while obtaining capacitance values comparable to the PVDF case. From these results, it is possible to conclude that

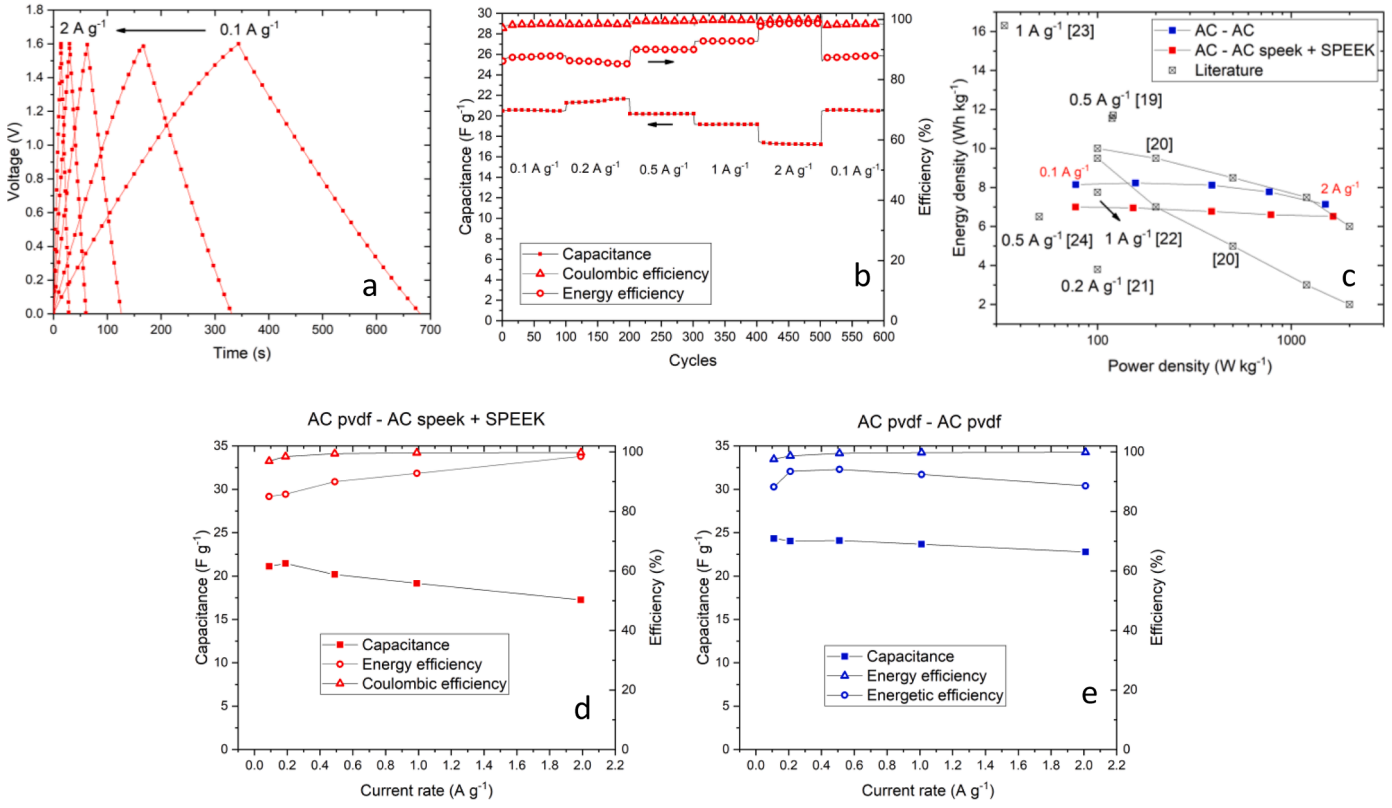

Fig. 8. Galvanostatic device measurements: a), b) measurements at different current rates for AC pvdf – AC speek + SPEEK device, c) comparison of device proposed with literature, d), e) comparison of device proposed with bare AC pvdf – AC pvdf device.

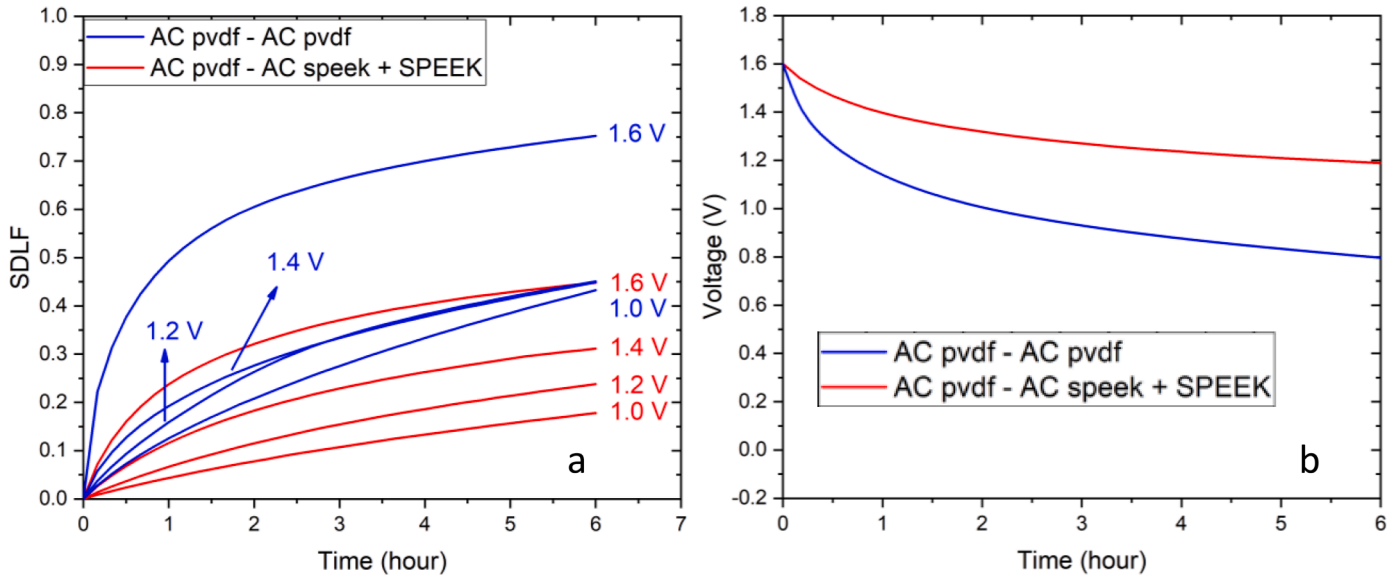

Fig. 9. a) Self discharge leakage factor comparison for the devices analyzed for all voltages, b) voltage profile in OCV conditions after 20 h float at 1.6 V.

the deposition of a conformal polymeric coating on top of the electrodes provides a reduction of the total capacitance of the electrode. This phenomenon is quite intuitive when considering that the polymer will partially fill some of the porosity of the AC, making them inaccessible for the ions. On the other hand, the replacement of the PVDF with the SPEEK ensures the reduction of the ESR and improves the capacitance. Therefore, by exploiting the combination of those contributions it is possible to obtain an electrode that shows the same capacitance as the AC pvdf electrode, but with a halved ESR and a higher coulombic efficiency (@ −1 V 98% vs 90%).

3.5. Device measurements

The 3-electrodes measurements allowed to study each material independently. When moving to the 2-electrodes measurements, the previous results came in handy to define which would be the best couple of materials to be paired. The electrochemical characterizations reported in Fig. 6b suggested that by applying an appropriate charge/mass balance it was possible to assemble a device working up to 1.6 V and maintain the coulombic efficiency above 98%, exploiting the AC speek + SPEEK as the negative electrode and the AC pvdf as the positive one. The electrodes' masses were balanced with the following relation [24]:

$$m_+C_+V_+ = m_-C_-V_-$$

Where C and V are the maximum capacitances and polarizations rated for a coulombic efficiency greater than 98%. By solving the above relation, it was found out that the correct mass ratio is $m_+/m_- = 1.8$.

3.5.1. Constant current charge and discharge

The devices were charged and discharged at in the operating window from 0 V up to 1.6 V using a constant current method. Different current rates were employed to verify the response of the devices and to test their cyclability and rate capability. The results are reported in Fig. 8.

What is possible to find out is that increasing the current rate, the SPEEK modified device show an increasing energy efficiency. AC based device and AC speek + SPEEK device start at 0.1 A g^{-1} current rate with a comparable energy efficiency, but in the first case, when reaching 1 A g^{-1}, the efficiency decreases below 90%, while in the second case, this is increased and it reaches about 95%. Considering the potential profile, it is clear how the behavior is linear and purely capacitive for the whole duration of the test. In Fig 8c, a Ragone plot is reported, comparing the behavior of AC pvdf device and AC speek + SPEEK device. Here is clear how the second device is able to reach higher values of power, by maintaining an almost constant ability to store energy, while the first one already starts to show a steep fold down. As a drawback, it can be observed that the energy density of SPEEK modified device remains lower than the one of the AC based one. This drawback was expected since an IEM on the top of an electrode will negatively affect the capacitance of the entire device and, therefore, the energy density. On the other hand, however, the membrane will produce benefits related to improved electrochemical stability and higher voltage window.

Moreover, some literature results are reported [25–30]: what comes out from the comparison is that the performances of here proposed device are comparable to the state of art. In addition, it is possible to notice that, in general, on equal current rates, this work ensures higher power densities at the same energy density with respect to the literature.

After the end of 2 A g^{-1} procedure, it was decided to repeat the 0.1 A g^{-1} current rate to confirm that the device performance was not affected by the cycling.

3.5.2. Self-discharge

Self-discharge (SD) tests were performed by applying different constant voltages for 20 h, and then letting the device relax for 6 h. In this way, by comparing the behaviors of the device without the IEM and the one with, it is possible to notice how SPEEK dramatically affects the performances by drastically reducing the self-discharge, as also confirmed through evaluation of self-discharge energy loss factor (SDLF). This factor was calculated as also reported in [31]:

$$SDLF = 1 - \left(\frac{V(t)}{V_f}\right)^2$$

Considering Fig. 9a, what stands out is that SPEEK provides a noticeable reduction of SD phenomenon. The trend for both devices is the same: when the floating voltage is increased, the SDLF increases too. Moreover it is evident how the leakage factor for AC based device drastically increases, raising the voltage from 1.4 V to 1.6 V, while the SPEEK based device, for the highest polarization imposed, shows a SDLF comparable with the lower polarization of the AC device. In fact, considering Fig. 9b, it is possible to appreciate how the red curve after 6 h of open circuit condition has lost 25% of its initial voltage, while the blue curve is 50% decreases comparing to the initial conditions.

3.5.3. Aging

The last test was the evaluation of the long-lasting performances of

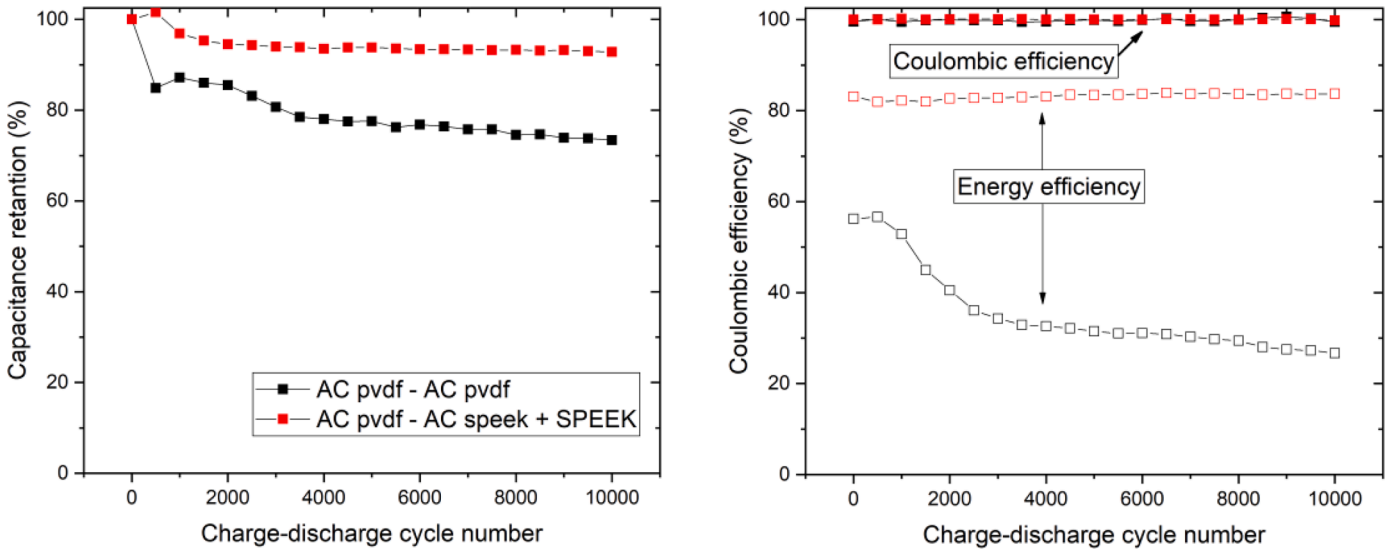

Fig. 10. a) Capacitance retention plot, b) coulombic and energy efficiency.

the devices. It was decided to perform 10,000 cycles at 1 A g^{-1} at the maximum operating voltage (1.6 V) and compare the results of the symmetric device made of AC pvdf. The results show a much higher capacitance retention, keeping 70% of the initial capacitance after 10,000 cycles. Interestingly, the symmetric device had a dramatic fall of the performance in the first 1000 cycles, keeping slowly decreasing its capacitance during the rest of the test. On the contrary, the device with the SPEEK slightly decreased its capacitance in first 2000 cycles, without any steep decrease, continuing preserving more than 90% of the initial capacitance (Fig. 10a).

Moreover, as shown in Fig. 10b, coulombic efficiency remains high for both devices for the 10,000 cycles, while the energy efficiencies (since the start) are very different: SPEEK modified device shows a much higher value (>80%), and it remains stable for the whole test, while symmetric device starts from 55% of energy efficiency and during the test, this value continues to decrease, reaching at last about 25%.

It has to be noticed that the capacitance retention and the energy efficiency does not lower at the same time. To understand this, a visual method was provided in [32]. Considering AC pvdf – AC pvdf device, in the first 500 cycle there was a steep reduction of the discharging time (increase of the slope, so reduction of the capacitance). After cycle 1000, iR drop start to rise, becoming more and more relevant, producing a lowering of the energy efficiency. Considering on the other hand, the AC pvdf – AC speek + SPEEK device, it experienced a reduction in the charging/discharging step time (reduction of the capacitance), while avoiding the rising up of a noticeable iR drop, which remained constant, letting the energy efficiency also to remain unaltered.

4. Conclusions

This study investigated the possibility of employ the SPEEK both as binder and IEM inside a supercapacitor. As IEM, the SPEEK was coated over the electrode with a very fast, simple and scalable approach, obtaining a thickness of less than 700 nm. Electrochemical characterizations proved how this coating is enhancing the performance of the single electrode, acting as a cation exchange: in particular the use of SPEEK allows to reduce by 50% the ESR value compared to bare AC electrode and at the same time to enhance the negative operating voltage window up to −1 V, maintaining coulombic efficiency over 98%. When employed in a device, it was possible to obtain a supercapacitor with an aqueous-based electrolyte working stably in a voltage window of 1.6 V, with a coulombic efficiency of 99%. The proposed strategy allows an improvement of the electrode/membrane interface with respect to previous works in the literature. The thin conformal membrane coating proved to be successful in reducing the impedance associated to that interface, while still performing efficiently as IEM. Moreover, the tiny amount of material required for the coating will impact positively the final cost of the device, compared to standard thick IEM.

CRediT authorship contribution statement

Davide Molino: Methodology, Investigation, Data curation, Writing – original draft, Visualization. **Alessandro Pedico:** Methodology, Investigation, Writing – original draft, Writing – review & editing. **Pietro Zaccagnini:** Methodology, Investigation, Writing – review & editing. **Sergio Bocchini:** Investigation, Writing – original draft, Writing – review & editing. **Andrea Lamberti:** Conceptualization, Writing – review & editing, Supervision.

Declaration of Competing Interest

The authors declare that they have no known competing financial interests or personal relationships that could have appeared to influence the work reported in this paper.

Data availability

Data will be made available on request.

Acknowledgment

This result is part of a project that has received funding from the European Research Council (ERC) under the European Union's ERC Starting Grant. Grant agreement "CO2CAP" No. 949916

Supplementary materials

Supplementary material associated with this article can be found, in the online version, at doi:10.1016/j.electacta.2023.143143.

References

[1] M.A. Shehzad, A. Yasmin, X. Ge, L. Wu, T. Xu, A Review of nanostructured ion-exchange membranes, Adv. Mater. Technol. 6 (2021), 2001171, https://doi.org/10.1002/admt.202001171.

[2] H. Strathmann, A. Grabowski, G. Eigenberger, Ion-exchange membranes in the chemical process industry, Ind. Eng. Chem. Res. 52 (2013) 10364–10379, https://doi.org/10.1021/ie4002102.
[3] Q. Wu, D. Liang, S. Lu, H. Wang, Y. Xiang, D. Aurbach, E. Avraham, I. Cohen, Advances and perspectives in integrated membrane capacitive deionization for water desalination, Desalination 542 (2022), 116043, https://doi.org/10.1016/j.desal.2022.116043.
[4] J.G. Hong, H. Gao, L. Gan, X. Tong, C. Xiao, S. Liu, B. Zhang, Y. Chen, Nanocomposite and nanostructured ion-exchange membrane in salinity gradient power generation using reverse electrodialysis. Advanced Nanomaterials for Membrane Synthesis and Its Applications, Elsevier, 2019, pp. 295–316, https://doi.org/10.1016/B978-0-12-814503-6.00013-6.
[5] X. Wang, R.S. Chandrabose, Z. Jian, Z. Xing, X. Ji, A 1.8V aqueous supercapacitor with a bipolar assembly of ion-exchange membranes as the separator, J. Electrochem. Soc. 163 (2016) A1853–A1858, https://doi.org/10.1149/2.0311609jes.
[6] T.A. Ibidapo, Classification of ionic polymers, Polym. Eng. Sci. 28 (1988) 1473–1476, https://doi.org/10.1002/pen.760282207.
[7] H. Strathmann, Chapter 2 - Electrochemical and Thermodynamic Fundamentals, in: H. Strathmann (Ed.) 9, 2004, pp. 23–88, https://doi.org/10.1016/S0927-5193(04)80033-0.
[8] L. Chen, H. Bai, Z. Huang, L. Li, Mechanism investigation and suppression of self-discharge in active electrolyte enhanced supercapacitors, Energy Environ. Sci. 7 (2014) 1750–1759, https://doi.org/10.1039/C4EE00002A.
[9] A.J. Paleo, P. Staiti, A. Brigandì, F.N. Ferreira, A.M. Rocha, F. Lufrano, Supercapacitors based on AC/MnO_2 deposited onto dip-coated carbon nanofiber cotton fabric electrodes, Energy Storage Mater. 12 (2018) 204–215, https://doi.org/10.1016/j.ensm.2017.12.013.
[10] X. Guo, M. Wang, J. Li, Y. Wei, K. Lian, J. Qiao, Multi-walled carbon nanotubes incorporation into cross-linked novel alkaline ion-exchange membrane for high efficiency all-solid-state supercapacitors, Int. J. Energy Res. 44 (2020) 4038–4047, https://doi.org/10.1002/er.5194.
[11] X. Cai, Y. Zhang, C. Li, G. Zhang, X. Wang, X. Zhang, Q. Wang, F. Wang, Composite polymer anion exchange membranes with sandwich structure and improved performance for Zn–Air battery, Membranes 11 (2021) 224, https://doi.org/10.3390/membranes11030224.
[12] R.K. Nagarale, G.S. Gohil, V.K. Shahi, Recent developments on ion-exchange membranes and electro-membrane processes, Adv. Colloid Interface Sci. 119 (2006) 97–130, https://doi.org/10.1016/j.cis.2005.09.005.
[13] K.D. Kreuer, On the development of proton conducting polymer membranes for hydrogen and methanol fuel cells, J. Memb. Sci. 185 (2001) 29–39, https://doi.org/10.1016/S0376-7388(00)00632-3.
[14] R. Yee, K. Zhang, B. Ladewig, The effects of sulfonated poly(ether ether ketone) ion exchange preparation conditions on membrane properties, Membranes 3 (2013) 182–195, https://doi.org/10.3390/membranes3030182.
[15] C. Zhao, H. Lin, K. Shao, X. Li, H. Ni, Z. Wang, H. Na, Block sulfonated poly(ether ether ketone)s (SPEEK) ionomers with high ion-exchange capacities for proton exchange membranes, J. Power Sources 162 (2006) 1003–1009, https://doi.org/10.1016/j.jpowsour.2006.07.055.
[16] A. Lamberti, M. Serrapede, G. Ferraro, M. Fontana, F. Perrucci, S. Bianco, A. Chiolerio, S. Bocchini, All-SPEEK flexible supercapacitor exploiting laser-induced graphenization, 2D Mater. 4 (2017) 035012. doi:10.1088/2053-1583/aa790e.
[17] S.S. Rajaputra, N. Pennada, A. Yerramilli, N.M. Kummara, Graphene based sulfonated polyvinyl alcohol hydrogel nanocomposite for flexible supercapacitors, J. Electrochem. Sci. Eng. 11 (2021) 197–207, https://doi.org/10.5599/JESE.1031.
[18] B. Karaman, A. Bozkurt, Enhanced performance of supercapacitor based on boric acid doped PVA-H_2SO_4 gel polymer electrolyte system, Int. J. Hydrogen Energy 43 (2018) 6229–6237, https://doi.org/10.1016/j.ijhydene.2018.02.032.
[19] B. Wang, X. Zhao, J. Liang, J. Liu, Y. Yang, M. Zhang, H. Yu, J. Li, Y. Tong, Q. Tang, Y. Liu, Microwave-Welded and photopolymer-embedded silver nanowire electrodes for skin-like supercapacitors, ACS Appl. Energy Mater. 5 (2022) 10490–10500, https://doi.org/10.1021/acsaem.2c01140.
[20] M. Drdácký, J. Lesák, S. Rescic, Z. Slížková, P. Tiano, J. Valach, Standardization of peeling tests for assessing the cohesion and consolidation characteristics of historic stone surfaces, Mater. Struct. 45 (2012) 505–520, https://doi.org/10.1617/s11527-011-9778-x.
[21] B. Li, H. Lopez-Beltran, C. Siu, K.H. Skorenko, H. Zhou, W.E. Bernier, M. S. Whittingham, W.E. Jones, Vaper phase polymerized PEDOT/cellulose paper composite for flexible solid-state supercapacitor, ACS Appl. Energy Mater. 3 (2020) 1559–1568, https://doi.org/10.1021/acsaem.9b02044.
[22] W. Chen, R.B. Rakhi, L. Hu, X. Xie, Y. Cui, H.N. Alshareef, High-performance nanostructured supercapacitors on a sponge, Nano Lett. 11 (2011) 5165–5172, https://doi.org/10.1021/nl2023433.
[23] S. Dsoke, X. Tian, C. Täubert, S. Schlüter, M. Wohlfahrt-Mehrens, Strategies to reduce the resistance sources on electrochemical double layer capacitor electrodes, J. Power Sources 238 (2013) 422–429, https://doi.org/10.1016/j.jpowsour.2013.04.031.
[24] V. Khomenko, E. Raymundo-Piñero, F. Béguin, Optimisation of an asymmetric manganese oxide/activated carbon capacitor working at 2V in aqueous medium, J. Power Sources 153 (2006) 183–190, https://doi.org/10.1016/j.jpowsour.2005.03.210.
[25] A.J. Paleo, P. Staiti, A.M. Rocha, G. Squadrito, F. Lufrano, Lifetime assessment of solid-state hybrid supercapacitors based on cotton fabric electrodes, J. Power Sources 434 (2019), 226735, https://doi.org/10.1016/j.jpowsour.2019.226735.
[26] S. Liu, T. Stettner, R. Klukas, T. Porada, K. Furda, A.M. Fernández, A. Balducci, Caesium acetate-based electrolytes for aqueous electrical double layer capacitors, ChemElectroChem 9 (2022) 1–7, https://doi.org/10.1002/celc.202200711.
[27] D. Jiménez-Cordero, F. Heras, M.A. Gilarranz, E. Raymundo-Piñero, Grape seed carbons for studying the influence of texture on supercapacitor behaviour in aqueous electrolytes, Carbon N.Y. 71 (2014) 127–138, https://doi.org/10.1016/j.carbon.2014.01.021.
[28] L.-F. Chen, Z.-H. Huang, H.-W. Liang, H.-L. Gao, S.-H. Yu, Three-dimensional heteroatom-doped carbon nanofiber networks derived from bacterial cellulose for supercapacitors, Adv. Funct. Mater. 24 (2014) 5104–5111, https://doi.org/10.1002/adfm.201400590.
[29] D. Hulicova-Jurcakova, A.M. Puziy, O.I. Poddubnaya, F. Suárez-García, J.M. D. Tascón, G.Q. Lu, Highly stable performance of supercapacitors from phosphorus-enriched carbons, J. Am. Chem. Soc. 131 (2009) 5026–5027, https://doi.org/10.1021/ja809265m.
[30] H. Wang, X. Sun, Z. Liu, Z. Lei, Creation of nanopores on graphene planes with MgO template for preparing high-performance supercapacitor electrodes, Nanoscale 6 (2014) 6577–6584, https://doi.org/10.1039/C4NR00538D.
[31] F. Soavi, C. Arbizzani, M. Mastragostino, Leakage currents and self-discharge of ionic liquid-based supercapacitors, J. Appl. Electrochem. (2014) 491–496, https://doi.org/10.1007/s10800-013-0647-x.
[32] P. Zaccagnini, A. Lamberti, A perspective on laser-induced graphene for micro-supercapacitor application, Appl. Phys. Lett. 120 (2022), https://doi.org/10.1063/5.0078707.